

Self-Templated Formation of Uniform F-CuO Hollow Octahedra for Lithium Ion Batteries

Zhongyuan Ma, Kun Rui, Qiao Zhang, Yao Zhang, Min Du, Desheng Li, Qingqing Wang, Xiao Huang,* Jixin Zhu,* and Wei Huang*

Owing to their intriguing properties such as structural versatility and good electrochemical reactivity, transition metal oxides (TMOs) have received tremendous research interest as electrodes for lithium ion batteries (LIBs) since Tarascon reported the first CoO-based conversion-type electrode for LIBs in 2000.^[1–3] With respect to the undesirable cycling stability associated with volume changes during Li uptaking and extraction, various nanostructured TMOs have been prepared, demonstrating much improved stability and thus much enhanced electrochemical performance.^[4,5] Among the various TMOs which are suitable anode materials for LIBs, cupric oxide (CuO) can deliver a large theoretical capacity of 674 mAh g⁻¹ via a two electron transfer process. In addition, by formation of hollow CuO nanostructures, much enhanced electrode kinetics and improved cycling stability can be achieved, due to reasons such as the increased interface area between electrode and electrolyte, reduced diffusion pathways for both Li⁺ and electrons, and improved accommodation of volume changes during the electrochemical process.^[6,7]

The morphologies of CuO nanocrystals can be well designed by controlling the kinetics of nucleation and growth through changing surfactants, solvents, temperature, etc. To construct hollow structured CuO, several strategies have been proposed, mainly involving the use of sacrificial templates

(e.g., organic complexes, hard templates) coupled with synthetic processes such as controllable Ostwald ripening process and heat treatment.^[8–14] Nevertheless, these procedures generally involve multiple steps, and mainly result in the preparation of spherical hollow structures. Cu₂O and CuO nanospheres can also be applied as templates for preparation of various types of transition metal compounds (e.g., metal oxides, metal hydroxides, and metal sulfides) hollow structures via different synthetic routes.^[15,16] However, fabrication of hollow structured CuO nanocrystals using itself as templates has been scarcely reported. In addition, the hollow structure of CuO endowed with typical traits such as well-defined morphology, surface area, and crystal facets exposure will promisingly contribute to enhanced Li storage performance. However, controllable construction of anisotropic hollow structures with nonspherical morphologies remains a big challenge.

Herein, the formation of unique hollow structures with designable structural features has been achieved via tunable structure-evolution reaction. Uniform hollow CuO octahedra doped with FeOOH (denoted as F-CuO hollow octahedra) have been fabricated via a facile self-templated method for the first time. The FeOOH hollow octahedra constructed with ultrathin nanosheets as ideal building blocks can also be fabricated by changing the reaction agent from deionized water to ethanol. Here, hollow structured octahedra with well-defined morphology and composition can be easily tuned with precise manipulation. Furthermore, the amorphous FeOOH doped hollow CuO octahedra used as anode materials demonstrate very good lithium storage properties. It is worth mentioning that this procedure can be extended to fabricate other nonspherical hollow structured CuO-based metal oxides.

Scheme 1 shows a schematic illustration for the overall synthetic process of the hollow octahedra. A typical process started with presynthesized Cu₂O solid octahedra as templates. After the Cu₂O octahedra were oxidized via annealing in air, the resulting CuO octahedra further underwent a hydrothermal/solvothermal treatment in the presence of FeCl₂. While F-CuO hollow octahedra can be obtained when ethanol was used as the solvent, FeOOH hollow octahedra constructed from sheet-like subunits can be obtained by simply altering the solvent from ethanol to water.

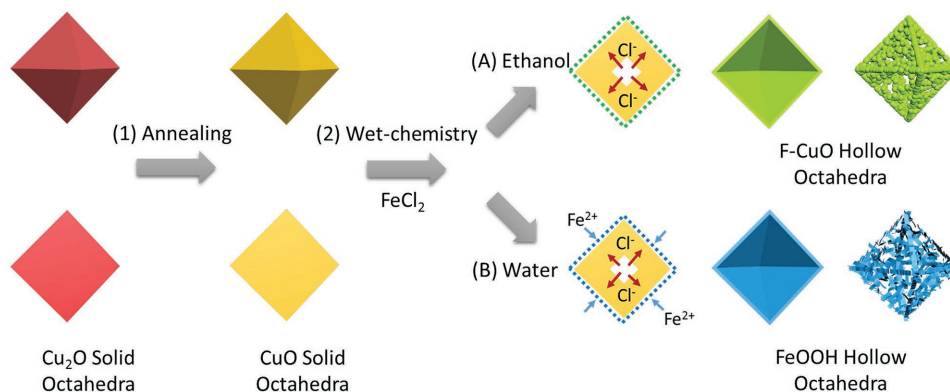
As seen from the field-emission scanning electron microscopy (FESEM) image in **Figure 1a**, uniformly dispersed

Z. Y. Ma, Dr. K. Rui, Q. Zhang, Y. Zhang, M. Du, D. S. Li, Q. Q. Wang, Prof. X. Huang, Prof. J. X. Zhu, Prof. W. Huang
Key Laboratory of Flexible Electronics (KLOFE) and Institute of Advanced Materials (IAM)
Jiangsu National Synergetic Innovation Center for Advanced Materials (SICAM)
Nanjing Tech University (NanjingTech)
30 South Puzhu Road, Nanjing 211816, China
E-mail: iamxhuang@njtech.edu.cn; iamjx Zhu@njtech.edu.cn; iamwhuang@njtech.edu.cn



Prof. W. Huang
Key Laboratory for Organic Electronics and Information Displays and Institute of Advanced Materials (IAM)
Jiangsu National Synergetic Innovation Center for Advanced Materials (SICAM)
Nanjing University of Posts and Telecommunications (NUPT)
9 Wenyuan Road, Nanjing 210023, China

DOI: 10.1002/sml.201603500



Scheme 1. Schematic illustration showing the formation of uniform F-CuO and FeOOH hollow octahedra. Stage 1: facile formation of CuO solid octahedra by directly annealing of Cu₂O template in air; Stage 2: FeCl₂ assisted etching process via a wet chemistry method; Stage 3: formation of F-CuO hollow octahedra by a) self-templated process and b) FeOOH hollow octahedra via structure-evolution reaction.

Cu₂O templates with an octahedral shape display an average edge length of ≈ 500 nm. After annealing, the octahedral morphology can still be observed for the resulting CuO particles (Figure 1b). A subsequent solvothermal treatment of the solid CuO in the presence of FeCl₂ led to the formation of hollow F-CuO with the preserved octahedral morphology (Figure 1c) but roughened surface as shown from the magnified FESEM image in Figure 1d. In contrast, the as-obtained FeOOH octahedra display fluffy surfaces that are likely constructed from nanosheet subunits (Figure 1e,f).

Transmission electron microscopy (TEM) analysis was further performed to examine the microstructure of the as-prepared octahedral samples. Solid CuO octahedra (Figure 2a) consist of numerous ≈ 5 nm CuO nanoparticles (Figure 2b,c). Based on the inset high-resolution transmission electron microscopy (HRTEM) image in Figure 2c, well-defined lattice fringes corresponding to interplanar spacings of 0.25 and 0.23 nm can be indexed to (002) and (200) planes of monoclinic CuO (JCPDS no. 48-1548), respectively. Figure 2d–f shows the morphological and structural analysis of hollow structured F-CuO octahedra, which were transformed successfully from solid CuO via the facile

solvothermal reaction in the presence of FeCl₂. The roughened surface seen in Figure 2d has been confirmed to be due to the aggregation of CuO nanoparticles (Figure 2e). HRTEM image in Figure 2f further indicates the polycrystalline nature of the hollow F-CuO with domain sizes less than 5 nm. Unambiguous lattice fringes (inset of Figure 2f) within a typical nanodomain correspond to lattice distances of 0.23 and 0.25 nm, in agreement with (200) and (002) planes of monoclinic CuO, respectively. It is worth mentioning that amorphous domains indicated by red circles in Figure 2f can also be detected. With this regard, iron related doping is speculated to be responsible and confirmed in the following parts. As characterized by N₂ adsorption–desorption measurement (Figure S1, Supporting Information), these F-CuO hollow octahedra possess a Brunauer–Emmett–Teller specific surface area as high as 70 m² g⁻¹, with the pore sizes mostly around 2 nm. When water was used as the solvent, a totally different hollow structure can be obtained. As shown in Figure 2g,h, hierarchical hollow octahedra with desirable interior voids are constructed from ultrathin FeOOH nanosheets, which are highly transparent to electron beam. The inset HRTEM image of a typical nanosheet lying perpendicularly

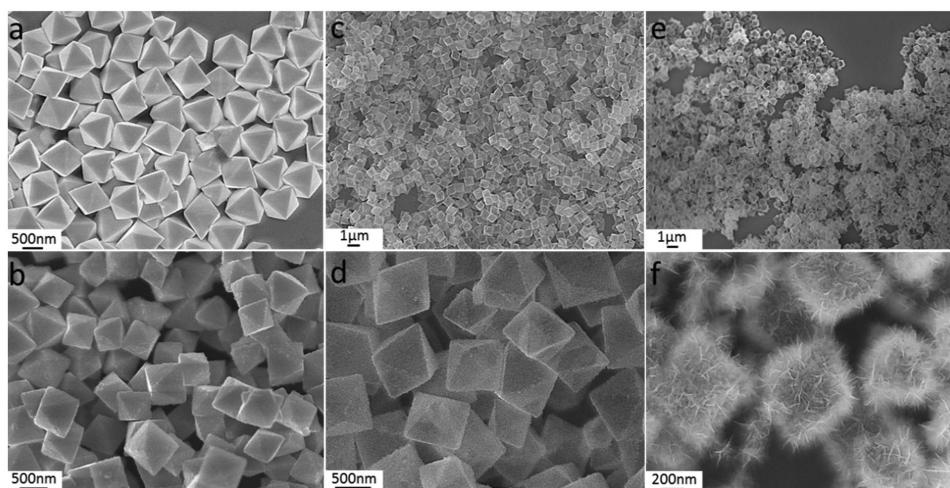


Figure 1. Typical field emission scanning electron microscopy (FESEM) images of a) Cu₂O solid octahedra, b) CuO solid octahedra, c,d) F-CuO hollow octahedra, and e,f) FeOOH hollow octahedra.

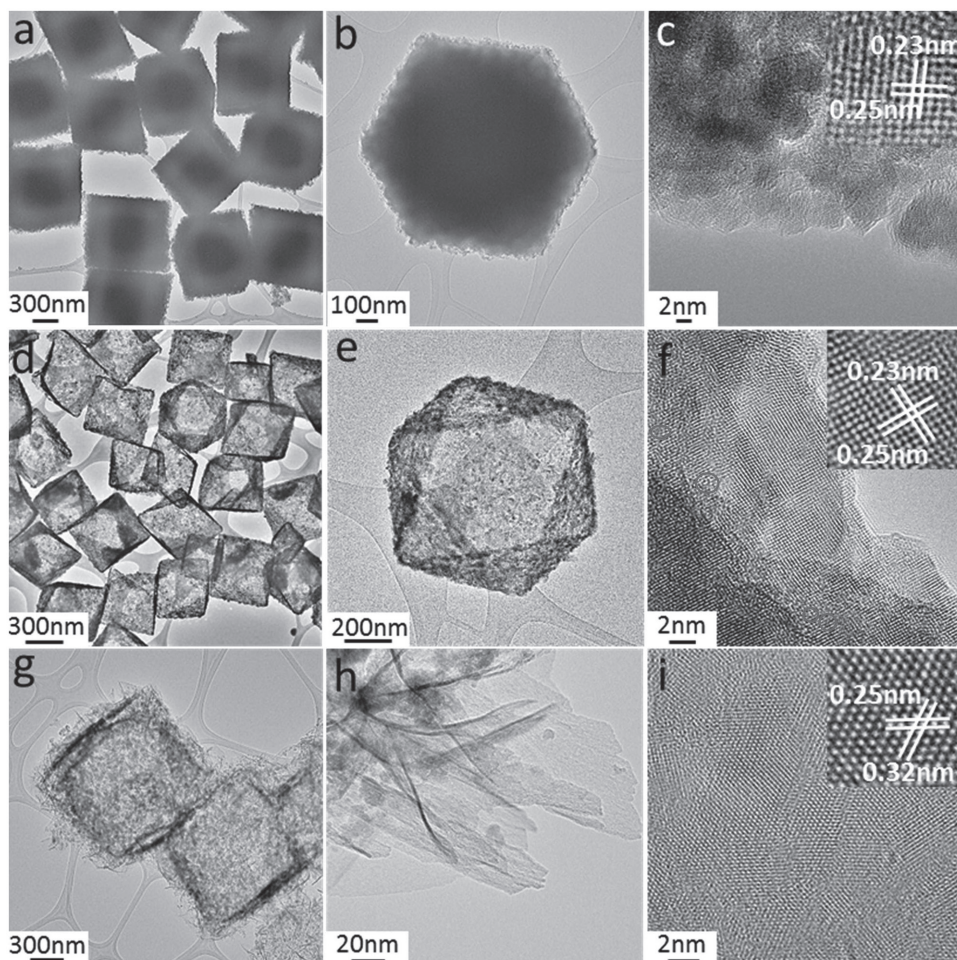


Figure 2. Typical transmission electron microscopy (TEM) images of a–c) CuO solid octahedra, d–f) F-CuO hollow octahedra, and g–i) FeOOH hollow octahedra. The insets of (c), (f), and (i) are corresponding high-resolution TEM images.

to the electron beam (Figure 2i) reveals interplane distances of 0.32 and 0.25 nm, in agreement with those of the (210) and (301) planes of orthorhombic FeOOH (JCPDS no. 44-1415), respectively.

The X-ray diffraction (XRD) patterns of as-prepared Cu₂O and CuO octahedra with solid and hollow structures are shown in **Figure 3a**. All the observed reflections of the presynthesized Cu₂O can be indexed according to the cubic structured Cu₂O (JCPDS no. 77-0199). As for both solid and hollow CuO octahedra, major diffraction peaks at 35.4°, 38.7°, and 48.7° can be assigned to (002)/(11-1), (111)/(200), and (20-2) reflections of CuO with the C2/c space group (JCPDS no. 48-1548), respectively. No impurity peaks belonging to Cu₂O were detected, suggesting the complete Cu₂O to CuO transition after annealing and subsequent solvothermal process. Moreover, broadened peaks for CuO crystals are observed, suggesting the existence of nanosized crystals as building blocks for the hierarchical architectures, in consistent with the TEM observation (Figure 2).

The chemical composition and oxidation states of the as-prepared hollow structured CuO were examined by X-ray photoelectron spectroscopy (XPS, Figure 3b–d). The high resolution Cu 2p spectrum in Figure 3b reveals two strong peaks at 933.9 and 953.8 eV corresponding to Cu 2p_{3/2} and

Cu 2p_{1/2} bands, respectively. Besides, satellites peaks at 941.3 and 943.7 eV for Cu 2p_{3/2}, and 962.3 eV for Cu 2p_{1/2} also reveal the Cu²⁺ state from the CuO phase.^[10,17] In addition, it is interesting to note that the XPS results in Figure 3c demonstrate the existence of element Fe in hollow structured CuO. As seen, the Fe peaks 2p_{3/2} at 710.9 eV and 2p_{1/2} at 725.0 eV can be assigned to FeOOH, accompanied by one satellite peak at 719.1 eV.^[18–20] Meanwhile, the appearance of the non-neglectable peak at around 713 eV provides evidence for the existence of Fe–O–Cu linkage in the F–CuO.^[21–23] In addition, the O 1s spectrum (Figure 3d) suggests the presence of Cu–O bond (529.9 eV), Fe–O–Fe (530.6 eV), and Fe–O–H (531.8 eV), and thus confirms the doping of Fe as FeOOH in CuO hollow octahedra. In this regard, the absence of FeOOH characteristic peaks in the XRD result evidences its amorphous feature. Elemental mapping based on energy-dispersive X-ray (EDX) spectroscopy (Figure S2, Supporting Information) has been performed to study the distribution of Cu, Fe, and O. The result provides clear information about the uniform distribution of Fe in the F-CuO hollow octahedra. Furthermore, trace Fe can also be verified by elemental analysis with inductively coupled plasma atomic emission spectroscopy (ICP-AES). The compositions of CuO hollow octahedra have been calculated accordingly

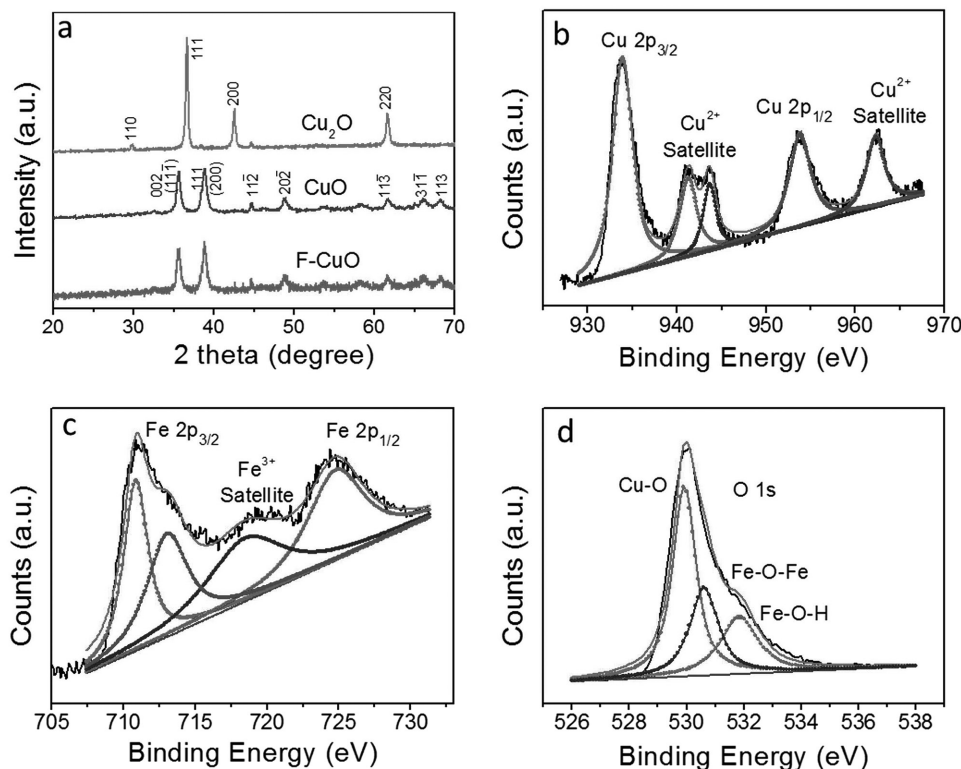


Figure 3. a) X-ray diffraction (XRD) patterns of Cu₂O solid octahedra, CuO solid octahedra, and F-CuO hollow octahedra. b–d) X-ray photoelectron spectroscopy (XPS) of F-CuO hollow octahedra, indicating the presence of Cu²⁺, Fe³⁺, and O²⁻ in the F-CuO hollow octahedra samples.

(Table S1, Supporting Information), and estimated to be CuO•FeOOH_{0.24}, which is therefore denoted as F-CuO in this work.

Based on the aforementioned characterization and analyses, we suggest that the coordination etching between the solid CuO template and Cl⁻ plays the key role in facilitating the formation of the hollow structured octahedra. For the solvothermal process with ethanol as the solvent, abundant Cl⁻ released from FeCl₂ would etch and coordinate with CuO, forming the soluble complex [CuCl_x]^{1-x} via an interfacial reaction.^[24] As a result, the solid CuO would gradually dissolve, leaving the octahedral template with an interior cavity. Meanwhile, in the presence of O₂ within the Teflon-lined autoclave, a slight alcoholysis of Fe²⁺ in ethanol not only enabled the possible precipitation of FeOOH nuclei, but also released protons (H⁺), contributing further to the etching of CuO. Taking into consideration the difficulty of alcoholysis of Fe²⁺ in ethanol, restricted nucleation and growth of FeOOH inhibited its crystallization, resulting in its amorphous feature and thus forming the FeOOH doped hierarchical CuO hollow octahedra eventually. In sharp contrast, when water was used as the solvent instead of ethanol, enhanced hydrolysis of Fe²⁺ would have occurred, contributing to an accelerated heterogeneous nucleation of FeOOH at the liquid–solid interface. In addition, more H⁺ ions would have been generated in water compared to in ethanol due to the promoted hydrolysis of Fe²⁺. Under the resultant acid environment, Cu-based phases such as Cu₂O, CuO, and Cu(OH)₂ could hardly remain, which is confirmed by XRD analysis (Figure S3, Supporting Information). Meanwhile, FeOOH

nuclei were gradually developed into highly crystalline 2D nanosheets, which is related to its intrinsic orthorhombic structure.^[25,26] While the FeOOH nanosheets grew in size to form the continuous shell, the original CuO template was completely etched under the dual influence of Cl⁻ and H⁺ to eventually yield the 3D hierarchical hollow structure.

The electrochemical performance of F-CuO hollow octahedra as anode for LIBs was investigated by a galvanostatic method. As displayed in **Figure 4a**, a reversible discharge capacity reaching 657 mAh g⁻¹ from the 2nd cycle onward is noted, approaching the theoretical values of pure CuO (674 mAh g⁻¹) and also F-CuO (723 mAh g⁻¹, calculated based on CuO•FeOOH_{0.24} as shown in Supporting information). After an activation process in the initial 50 cycles, the F-CuO anode then exhibits a stable cycling behavior with an activated capacity retained at 785 mAh g⁻¹ for the rest 50 cycles. It should be noted that this high reversible capacity exceeding the theoretical value of F-CuO (723 mAh g⁻¹, calculated based on CuO•FeOOH_{0.24}) can be attributed to the formation/deformation of solid electrolyte interface (SEI) layers and interfacial storage.^[27–29] In comparison, both solid CuO and Cu₂O octahedra anodes display an obvious capacity decay with remaining capacities of merely 69 and 45 mAh g⁻¹ after 100 cycles under the same conditions, respectively. Moreover, the FeOOH hollow octahedra delivered a reversible capacity of ≈740 mAh g⁻¹ at a current density of 0.5 A g⁻¹, as shown in Figure S4 (Supporting Information). Representative cyclic voltammograms further reveal the reaction mechanism of F-CuO anode (Figure S5, Supporting Information). During the first scan, the reduction peak at ≈2.0 V in the cathodic

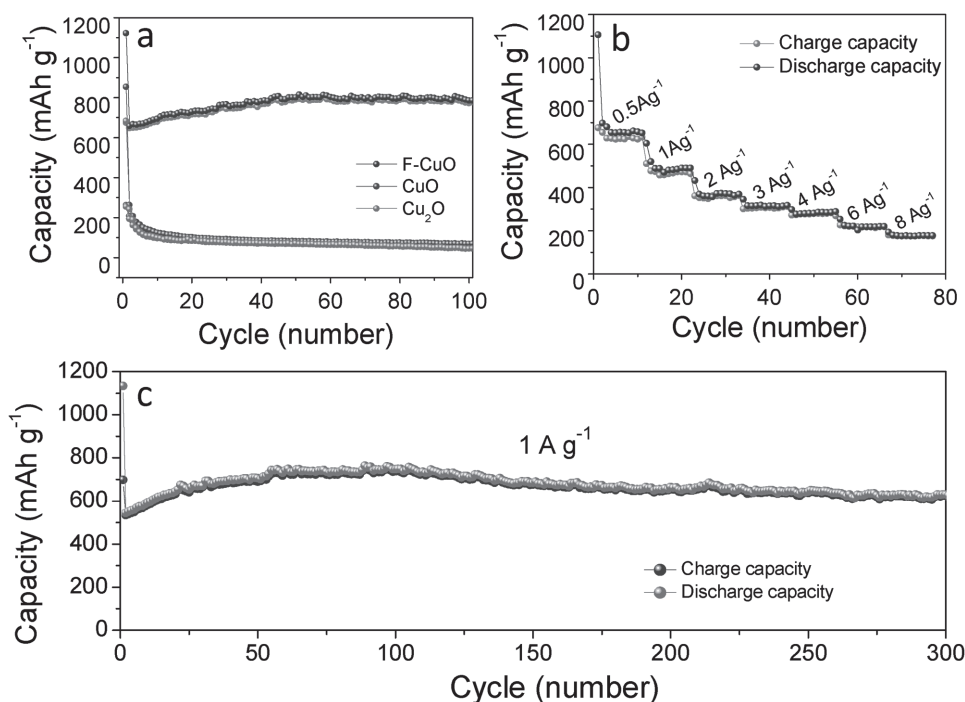


Figure 4. Electrochemical performances of a) cycling performance of Cu₂O solid octahedra, CuO solid octahedra, and F-CuO hollow octahedra at a current density of 500 mA g⁻¹. b) The rate-capability of F-CuO hollow octahedra at current densities from 500 to 8000 mA g⁻¹. c) Cycling performance of F-CuO hollow octahedra at a current density of 1000 mA g⁻¹.

sweep can be ascribed to the possible Li-intercalation process of amorphous FeOOH.^[27,28,30,31] Consistent with previous reports,^[11,32] another two main reduction peaks at ≈ 1.0 and 0.6 V can be assigned to the formation of intermediate Cu₂O upon the initial Li insertion and its further transformation into metallic Cu in Li₂O matrix, respectively. In sequent scans, the shift of cathodic peaks toward higher potentials is observed, corresponding to structure changes within metal oxides after conversion reactions. Yet, anodic peaks basically maintained at 1.7 and 2.5 V suggesting the oxidation of Cu into Cu₂O and further CuO afterward.

Rate performance of the F-CuO hollow octahedra anode was also examined at different current densities from 0.5 A g⁻¹ to as high as 8 A g⁻¹ (Figure 4b). As seen, reversible capacities of about 657 mAh g⁻¹ at 0.5 A g⁻¹, 488 mAh g⁻¹ at 1 A g⁻¹, 370 mAh g⁻¹ at 2 A g⁻¹, 315 mAh g⁻¹ at 3 A g⁻¹, 285 mAh g⁻¹ at 4 A g⁻¹, 218 mAh g⁻¹ at 6 A g⁻¹, and 177 mAh g⁻¹ at 8 A g⁻¹ can be obtained, respectively. A good overlapping of discharge and charge capacities during the test, especially at high current densities at 4–8 A g⁻¹, demonstrates the decent reversibility for Li storage reaction of F-CuO electrode, along with excellent coulombic efficiency approaching 100% under rapid charging/discharging process. For further evaluation of long cyclic performance, the F-CuO hollow octahedra anode was measured at 1 A g⁻¹ for 300 cycles (Figure 4c). A gradual capacity increase can also be observed from 543 mAh g⁻¹ after the initial capacity loss, all the way up to 747 mAh g⁻¹ around 60 cycles, after which the reversible capacity stabilized for another 40 cycles without distinct capacity fading. As has been discovered in other metal oxide electrodes, the progressive generation of polymeric gel-like films (e.g., SEI layer), which are electrochemically active, gives rise to

the capacity activation phenomenon.^[33–35] The resulting surface-related capacity grows until the completion of SEI formation, which contributes to the total reversible capacity along with the conversion-related capacity. Remarkably, the retained capacity as high as 624 mAh g⁻¹ after 300 cycles can be achieved. The excellent cycling stability of F-CuO in such a long term further confirms the structural superiority of hollow octahedra.

Therefore, noteworthy features of F-CuO hollow octahedra responsible for its superior cycling performance can be summarized as follows. First, due to the sufficient void space within the porous shell, hollow octahedral shell can stand repeated volume swing during the Li insertion/extraction reactions, enhancing the cycling stability effectively and somehow mitigating the pulverization. Second, delicate assembly of CuO nanoparticles into hierarchical structure not only ensures the large electrochemical active surface area facilitating electron/Li⁺ diffusion, but also benefits easy penetration of electrolyte, yielding improved rate capability. Moreover, the Li-intercalation of amorphous FeOOH would occur at a relative higher voltage (≈ 1.0 – 2.0 V) than CuO (≈ 0.2 – 1.0 V), which could be lithiated with volume changes first and contribute a portion of lithium storage.^[26] During the subsequent Li-insertion process of CuO at lower voltages, the resulting discharge products of FeOOH would in turn act as barriers to further restrain the volume expansion and aggregation of CuO nanoparticles. Therefore, the effective doping of amorphous FeOOH not only gives rise to the observed extra capacities, but also favors the cycling stability of CuO-based anode.

Herein, distinct advantages of this self-templated method can be summarized. By just changing the reaction time or agent,

the composition and structure of nonspherical hollow structures (from CuO to FeOOH doped CuO and pure FeOOH) can be easily tuned along with their building blocks (from nanoparticles to ultrathin nanosheets). In addition, with easily removable FeCl₂ salt offering Fe²⁺ for FeOOH doping and Cl⁻ for coordination etching, neither surfactants are used to direct the formation of hollow structures nor complicated post-treatments are required for our method here. Note that this presented procedure is a general approach, which can be extended to fabricate other nonspherical hollow structured metal oxides. For instance, by replacing the CuO solid octahedra with 1D solid nanowires, uniform F-CuO hollow nanotubes as well as FeOOH hollow nanotubes can be prepared with a similar FeCl₂ assisted etching approach. As illustrated by FESEM images (Figure S6, Supporting Information), both 1D tubular F-CuO and FeOOH exhibit roughened surface as compared to the CuO template. TEM images (Figure S7, Supporting Information) further show that a nanotube with the hollow interior is assembled from ultrathin CuO nanosheets. The corresponding elemental mapping (Figure S8, Supporting Information) indicates the co-existence of Fe with CuO, similar to the case of F-CuO hollow octahedra. Sustained lithium storage performance was also obtained for the self-supported electrode of F-CuO hollow nanotubes (Figure S9, Supporting Information). A reversible capacity of ≈ 1.12 mAh cm⁻² can be achieved after 60 cycles at a current density of 0.5 A cm⁻². Similarly, the microstructural traits of FeOOH nanotubes composed by nanosheet subunits were also confirmed by TEM (Figure S10, Supporting Information).

In summary, a new hollow structure of F-CuO octahedra has been fabricated via a facile self-templated wet chemistry method. It is found that a delicate control of reaction agents has an important influence on the composition and morphology of the product. When utilized as anodes in LIBs, the amorphous FeOOH doped hollow CuO octahedra demonstrate very good lithium storage properties, delivering a large reversible capacity as high as 624 mAh g⁻¹ at 1 A g⁻¹, even after 300 cycles. It is worth mentioning that this procedure can be extended to fabricate other nonspherical hollow structured CuO-based metal oxides.

Experimental Section

Preparation of Cu₂O Solid Octahedra: 8.88 g polyvinylpyrrolidone (PVP) (*M_w*: 40 000) was dissolved in 100 mL deionized water and 0.85 g CuCl₂ was added into the solution, which was kept at 50–55 °C under stirring. 4.0 g NaOH was dissolved in 20 mL deionized water and then added into above mixture to form a black solution. A mixture of 5.26 g ascorbic acid and 20 mL deionized water was added into the black solution afterward and stirred for 3 h at 55 °C. Finally, the Cu₂O octahedra were collected after washing by deionized water and ethanol.

Preparation of CuO Solid Octahedra: The as-prepared Cu₂O octahedra sample was heated at 300 °C in air for 60 min.

Preparation of F-CuO Hollow Octahedra: 50 mg CuO octahedra sample was dispersed in 40 mL 99.9% ethanol and then 50 mg of FeCl₂ was added into the solution. The mixture was sealed

in a 45 mL Teflon-lined autoclave and maintained at 170 °C for 60 min. After the reaction, the final products were cooled down to room temperature and the precipitates were collected followed by washing with deionized water and ethanol.

Preparation of FeOOH Hollow Octahedra: 50 mg CuO octahedra sample was dispersed in 40 mL deionized water together with an addition of 50 mg of FeCl₂ and put into 45 mL Teflon-lined autoclave. The mixture was maintained at 170 °C for 60 min and the final products were collected after washing by deionized water and ethanol several times.

Preparation of CuO Nanowire Arrays: A piece of copper foil with a typical dimension of 10 mm × 10 mm (Super Conductor Materials, 1 mm thick, 99.9%) was heated on a hot plate in air for 2 d.

Preparation of F-CuO and FeOOH Hollow Tubes: A piece of CuO nanowires sample with a dimension of 5 mm × 5 mm was dispersed in 40 mL 99.9% ethanol or deionized water together with an addition of 50 mg of FeCl₂ and transferred into 45 mL Teflon-lined autoclave. The mixture was maintained at 170 °C for 60 min and the final products were collected after washing by deionized water and ethanol several times.

Characterization: The morphologies of the samples were investigated by using a FESEM (JEOL, JSM-7600F). The nanostructures of the samples were characterized by using a TEM (JEOL, JEM-2100) operating at 200 kV. Crystal phases of the samples were identified using a X-ray power diffractometer (Scintag PAD-V) with Cu K α irradiation. XPS was carried out on the PHI Quantera X-ray photoelectron spectrometer. The elemental analysis of F-CuO hollow octahedra sample was performed by ICP-AES.

Electrochemical Measurements: For the working electrode preparation,^[36] 80 wt% of the as-prepared active materials (e.g., Cu₂O solid octahedra, CuO solid octahedra, F-CuO hollow octahedra, and FeOOH hollow octahedra), 10 wt% carbon black (Super-P), and 10 wt% polyvinylidene fluoride binder were mixed into *N*-methyl-2-pyrrolidinone solvent. The obtained slurry was coated onto Cu foil disks uniformly, which were then dried in vacuum at 50 °C for 12 h to remove the solvent. Lithium ion battery assembly was carried out on the CR2032 coin-type cells with lithium metal as the counter/reference electrode, Celgard 2400 membrane as the separator, and electrolyte obtained by dissolving 1 M LiPF₆ into a mixture of ethylene carbonate (EC) and dimethyl carbonate (DMC) (EC/DMC, 1:1, v/v). The coin cells were assembled in an Ar-filled glove-box with concentrations of moisture and oxygen below 1.0 ppm. The cyclability and rate-capability of Cu₂O solid octahedra, CuO solid octahedra, F-CuO hollow octahedra, and FeOOH hollow octahedra were performed with a NEWARE battery tester at a voltage window of 0.01–3.0 V. Cyclic voltammetry (0.01–3 V, 0.2 mV s⁻¹) was carried out on a CHI 660C electrochemical workstation.

Supporting Information

Supporting Information is available from the Wiley Online Library or from the author.

Acknowledgements

Z.M. and K.R. contributed equally to this work. This work was financially supported by the National Natural Science Foundation of China (No. 21501091 and No. 51322202), the Recruitment Program of Global Experts, National Key Basic Research Program of China (973) (2015CB932200), and NanjingTech Start-up Grant (3983500170).

-
- [1] M. V. Reddy, G. V. S. Rao, B. V. R. Chowdari, *Chem. Rev.* **2013**, *113*, 5364.
- [2] P. Poizot, S. Laruelle, S. Grugeon, L. Dupont, J. Tarascon, *Nature* **2000**, *407*, 496.
- [3] S. H. Yu, S. H. Lee, D. J. Lee, Y. E. Sung, T. Hyeon, *Small* **2016**, *12*, 2146.
- [4] B. L. Ellis, P. Knauth, T. Djenizian, *Adv. Mater.* **2014**, *26*, 3368.
- [5] C. Z. Yuan, H. B. Wu, Y. Xie, X. W. Lou, *Angew. Chem. Int. Ed.* **2014**, *53*, 1488.
- [6] X. W. Lou, L. A. Archer, Z. Yang, *Adv. Mater.* **2008**, *20*, 3987.
- [7] Z. Wang, L. Zhou, X. W. David Lou, *Adv. Mater.* **2012**, *24*, 1903.
- [8] C. C. Yec, H. C. Zeng, *J. Mater. Chem. A* **2014**, *2*, 4843.
- [9] J. Liu, D. Xue, *Adv. Mater.* **2008**, *20*, 2622.
- [10] C. Kong, L. Tang, X. Zhang, S. Sun, S. Yang, X. Song, Z. Yang, *J. Mater. Chem. A* **2014**, *2*, 7306.
- [11] R. Wu, X. Qian, F. Yu, H. Liu, K. Zhou, J. Wei, Y. Huang, *J. Mater. Chem. A* **2013**, *1*, 11126.
- [12] G. Jian, L. Liu, M. R. Zachariah, *Adv. Funct. Mater.* **2013**, *23*, 1341.
- [13] Y. Hu, X. Huang, K. Wang, J. Liu, J. Jiang, R. Ding, X. Ji, X. Li, *J. Solid State Chem.* **2010**, *183*, 662.
- [14] S. Gao, S. Yang, J. Shu, S. Zhang, Z. Li, K. Jiang, *J. Phys. Chem. C* **2008**, *112*, 19324.
- [15] S. Sun, Z. Yang, *Chem. Commun.* **2014**, *50*, 7403.
- [16] Z. Y. Wang, D. Y. Luan, C. M. Li, F. B. Su, S. Madhavi, F. Y. C. Boey, X. W. Lou, *J. Am. Chem. Soc.* **2010**, *132*, 16271.
- [17] W. Guo, W. Sun, Y. Wang, *ACS Nano* **2015**, *9*, 11462.
- [18] J. Liu, M. Zheng, X. Shi, H. Zeng, H. Xia, *Adv. Funct. Mater.* **2016**, *26*, 919.
- [19] J. X. Feng, S. H. Ye, H. Xu, Y. X. Tong, G. R. Li, *Adv. Mater.* **2016**, *28*, 4698.
- [20] Q. Yu, X. Meng, T. Wang, P. Li, J. Ye, *Adv. Funct. Mater.* **2015**, *25*, 2686.
- [21] G. K. Pradhan, K. M. Parida, *J. Ind. Eng. Chem.* **2012**, *18*, 1612.
- [22] Y. Li, M. Xu, L. Pan, Y. Zhang, Z. Guo, C. Bi, *J. Appl. Phys.* **2010**, *107*, 113908.
- [23] H. Dendaas, M. Passacantando, L. Lozzi, S. Santucci, P. Picozzi, *Surf. Sci.* **1994**, *317*, 295.
- [24] Z. Y. Wang, D. Y. Luan, F. Y. C. Boey, X. W. Lou, *J. Am. Chem. Soc.* **2011**, *133*, 4738.
- [25] Y. Chen, Y. Lin, Y. Hsu, S. Yen, K. Chen, L. Chen, *Small* **2014**, *10*, 3803.
- [26] J. Kim, U. G. Nielsen, C. P. Grey, *J. Am. Chem. Soc.* **2008**, *130*, 1285.
- [27] L. H. Yu, S. B. Xi, C. Wei, W. Y. Zhang, Y. H. Du, Q. Y. Yan, Z. C. Xu, *Adv. Energy Mater.* **2015**, *5*, 1501517.
- [28] Y. Song, Y. Cao, J. Wang, Y. N. Zhou, F. Fang, Y. S. Li, S. P. Gao, Q. F. Gu, L. F. Hu, D. L. Sun, *ACS Appl. Mater. Interfaces* **2016**, *8*, 21334.
- [29] T. Tabuchi, Y. Katayama, T. Nukuda, Z. Ogumi, *J. Power Sources* **2009**, *191*, 636.
- [30] X. Wang, X. Chen, L. Gao, H. Zheng, M. Ji, C. Tang, T. Shen, Z. Zhang, *J. Mater. Chem.* **2004**, *14*, 905.
- [31] K. Amine, H. Yasuda, M. Yamachi, *J. Power Sources* **1999**, *81*, 221.
- [32] A. Banerjee, U. Singh, V. Aravindan, M. Srinivasan, S. Ogale, *Nano Energy* **2013**, *2*, 1158.
- [33] F. Zou, X. Hu, Z. Li, L. Qie, C. Hu, R. Zeng, Y. Jiang, Y. Huang, *Adv. Mater.* **2014**, *26*, 6622.
- [34] J. Wang, Q. Zhang, X. Li, B. Zhang, L. Mai, K. Zhang, *Nano Energy* **2015**, *12*, 437.
- [35] Z. Wang, D. Luan, S. Madhavi, Y. Hu, X. W. Lou, *Energy Environ. Sci.* **2012**, *5*, 5252.
- [36] J. Zhu, Z. Lu, M. O. Oo, H. H. Hng, J. Ma, H. Zhang, Q. Yan, *J. Mater. Chem.* **2011**, *21*, 12770.

Received: October 18, 2016
Revised: November 12, 2016
Published online: